

# ***HST* CALSPEC FLUX STANDARDS: SIRIUS (AND VEGA)**

R. C. Bohlin

Space Telescope Science Institute, 3700 San Martin Drive, Baltimore, MD 21218

`bohlin@stsci.edu`

Received \_\_\_\_\_;    accepted \_\_\_\_\_

## ABSTRACT

The Space Telescope Imaging Spectrograph (STIS) has measured the flux for Sirius from 0.17–1.01  $\mu\text{m}$  on the *HST* White Dwarf scale. Because of the cool debris disk around Vega, Sirius is commonly recommended as the primary IR flux standard. The measured STIS flux agrees well with predictions of a special Kurucz model atmosphere, adding confidence to the modeled IR flux predictions. The IR flux agrees to 2–3% with respect to the standard template of Cohen and to 2% with the MSX absolute flux measurements in the mid-IR. A weighted average of the independent visible and mid-IR absolute flux measures implies that the monochromatic flux at 5557.5 Å (5556 Å in air) for Sirius and Vega, respectively, is  $1.35 \times 10^{-8}$  and  $3.44 \times 10^{-9}$   $\text{erg cm}^{-2} \text{ s}^{-1} \text{ Å}^{-1}$  with formal uncertainties of 0.5%. Contrary to previously published conclusions, the Hipparcos photometry offers no support for the variability of Vega. Pulse pileup severely affects the Hp photometry for the brightest stars.

*Subject headings:* circumstellar matter — stars:individual(Sirius, Vega) — stars:fundamental parameters (absolute flux) — techniques:spectroscopic

## 1. INTRODUCTION

Precise stellar flux standards are required for the calibration of the James Webb Space Telescope (JWST) and for the interpretation of dark energy measures with the supernova Ia technique. Cohen et al. (1992a) and, more recently, Engelke et al. (2010, EPK) recommend the use of Sirius as the primary IR standard, because Vega’s rapid rotation and dust ring complicate the modeling of its IR flux distribution. Thus, Sirius ( $\alpha$  CMa, HD 48915, HR 2491) was observed by *HST/STIS* on 2012 Oct 7 and 2013 Jan 26. The hot WD companion, Sirius B, is 10 mag fainter at V and contributes <1% of the system flux, even at 1300 Å (Holberg et al. 1998, Beuermann et al. 2006).

The HST flux system (Bohlin & Gordon 2014) is based on the flux distribution of NLTE model atmospheres for the pure hydrogen white dwarfs (WDs) GD153 and GD71 and on a NLTE metal line-blanketed model of Rauch et al. (2013, RWBK) for G191B2B. The absolute normalization of each model flux is defined by the STIS net signal in electrons/s from each WD relative to the STIS net signal for Vega at 5557.5 Å (5556 Å in air), where Megessier (1995) found an absolute flux of  $3.46 \times 10^{-9} \text{ erg cm}^{-2} \text{ s}^{-1} \text{ Å}^{-1} \pm 0.7\%$ . This paper reconciles the Megessier visible flux with the MSX mid-IR fluxes and derives  $3.44 \times 10^{-9} \text{ erg cm}^{-2} \text{ s}^{-1} \text{ Å}^{-1} \pm 0.5\%$  at 5556 Å for Vega’s monochromatic flux. This 0.6% change to the HST fluxes also brings the extrapolated flux for Sirius to within 0.6% of the average MSX mid-IR absolute flux measures.

The STIS Sirius observations and their flux calibration are discussed in Section 2. Section 3 compares the modeled IR spectral energy distribution (SED) with the MSX absolute flux measurements, while Section 4 discusses Vega, its dust rings, and the lack of any evidence for variability in the Hipparcos data.

## 2. CALIBRATION OF THE SATURATED OBSERVATIONS

STIS observations of Sirius in the three CCD low dispersion modes G230LB, G430L, and G750L (Hernandez 2012) heavily saturate the full well depth of the CCD detector. However, the excess charge just bleeds into adjacent pixels along the columns perpendicular to the dispersion axis and is not lost at Gain = 4. Gilliland et al. (1999, GGK) demonstrated that saturated signals on the STIS CCD are linear in total charge vs. stellar flux, as long as the extraction region on the image is large enough to include all the charge. In particular, GGK demonstrated linearity to 0.1% accuracy using  $50\times$  overexposed images of a star in M67 compared with unsaturated exposures of the same star.

Sirius data extraction and calibration proceeded as detailed for similarly saturated observations of Vega (Bohlin & Gilliland 2004, BG), except that taller extraction heights of 206, 182, and 148 pixels are required for G230LB, G430L, and G750L, respectively, for single 4s exposures with G230LB and 0.3s for G430L and G750L. For these saturated images, the signal level is so high that any signal loss due to charge transfer efficiency (CTE) effects (Goudfrooij & Bohlin 2006) is  $<0.1\%$ .

Table 1 is the journal of the Sirius observations, while Figure 1 demonstrates both the repeatability of G230LB observations and the linearity beyond saturation. The individual sub-exposure times from Table 1 are either 0.3s or 4s. Figure 1 shows the ratio of the six G230LB observations to their average. The two 16s exposures with four sub-exposures of 4s repeat to 0.2% and dominate the average spectrum. The 0.3s exposures average 0.30% higher than the 4s exposures, in agreement with BG, who also found 0.3009s for the nominal 0.3s exposure time. However, the scatter of  $\sigma = 0.17\%$  means that the 0.30% exposure time increase has less than a  $2\sigma$  significance; and 0.3000s is used for the short exposure time.

After extracting the spectra from the images, adjusting the flux to a standard 7-pixel-high aperture (Bohlin 1998), and correcting for sensitivity changes with time using

the method of Stys et al. (2004), corrections to the wavelengths are made for sub-pixel wavelength errors that are obvious in the high S/N saturated spectra. These shifts range up to 0.79 pixel and are found by cross-correlation of the absorption lines with a model flux distribution.

### 2.1. The new Rauch Flux Calibration

The STIS absolute flux calibration is based on model atmosphere SEDs for the three primary WDs G191B2B, GD153, and GD71. Gianninas et al. (2011, G11) fit new Balmer line observations of these WDs with updated NLTE, pure-hydrogen models that include improved theoretical calculations of the Balmer lines (Tremblay & Bergeron 2009). G11 found  $T_{\text{eff}}$  and  $\log g$  of 60920 K and  $7.55 \text{ cm s}^{-2}$  for G191B2B, 40320 K and  $7.93 \text{ cm s}^{-2}$  for GD153, and 33590 K and  $7.93 \text{ cm s}^{-2}$  for GD71. For G191B2B, RWBK computed line-blanketed NLTE models and reported a best fit to the absorption lines in STIS and FUSE high dispersion spectra of  $T_{\text{eff}} = 60000 \pm 2000 \text{ K}$  and  $\log g = 7.60$ . However, a  $T_{\text{eff}} = 59000 \text{ K}$  model is within the uncertainty and is more consistent with the STIS relative UV flux among the three stars. In addition, RWBK found  $N(HI) = 2.2 \times 10^{18} \text{ atoms cm}^{-2}$  from the Lyman lines, which corresponds to  $E(B-V)=0.0005$  according to the galactic average  $N(HI)/E(B-V) = 4.8 \times 10^{21} \text{ atoms cm}^{-2} \text{ mag}^{-1}$  of Bohlin et al. (1978).

New models for the three fundamental primary standards GD71, GD153, and G191B2B (Bohlin 2003) are calculated with the Tübingen NLTE Model-Atmosphere Package (Werner et al. 2003, Rauch & Deetjen 2003), which includes metal line blanketing for G191B2B but only pure hydrogen for GD153 and GD71 at the G11  $T_{\text{eff}}$  and  $\log g$ . The model parameters for the three primary WDs appear in Table 2. Their SEDs are available via CALSPEC<sup>1</sup>

---

<sup>1</sup><http://www.stsci.edu/hst/observatory/crds/calspec.html>

and also from the registered Virtual Observatory service TheoSSA<sup>2</sup> that was created in the framework of the GAVO<sup>3</sup> project. After reddening the G191B2B model by  $E(B-V)=0.0005$  and normalizing relative to the 5556 Å flux of for Vega, these three SEDs define the STIS absolute flux calibration and all observed STIS fluxes.

Previous to November 2013, pure hydrogen models calculated with the Hubeny NLTE code defined the SEDs of all three stars. The switch to Rauch models results in a wavelength dependent shift of the HST flux scale by  $<\sim 1\%$  in the STIS wavelength range. At 8  $\mu\text{m}$ , the worst discrepancy with the Spitzer/IRAC fluxes (Bohlin et al. 2011) had been a  $4\sigma$  difference of 12% for G191B2B. The 4% lower flux at 8  $\mu\text{m}$  for the new G191B2B SED reduces the discrepancy to 8% with less than a  $3\sigma$  significance.

The final Sirius fluxes adjusted to the new calibration can be found in the CALSPEC database with the file name sirius\_stis\_001.fits. Included in the file are the estimated systematic uncertainty of 1% and the statistical uncertainties, which determine a S/N per pixel that ranges up to 15000 at 4000-4100 Å, where  $2.4 \times 10^8$  electrons per pixel are extracted from the CCD spectral images.

---

<sup>2</sup>Theoretical Stellar Spectra Access, <http://dc.g-vo.org/theossa>

<sup>3</sup>German Astrophysical Virtual Observatory, <http://www.g-vo.org>

### 3. COMPARISON OF THE STIS FLUX FOR SIRIUS WITH MODELS AND OTHER RESULTS

#### 3.1. Kurucz, CWW, and EPK Models

Figure 2 compares the STIS flux for Sirius to other results, including an  $R = 500$  resolution, original Kurucz model<sup>4</sup> and an update (Kurucz private comm. 2013). All of the illustrated SEDs have been divided by the same theoretical smooth continuum, as normalized to the STIS flux at 6800–7700 Å, in order to display the spectral features on an expanded scale. Ratio plots of STIS/model have large and distracting, spurious dips and spikes near strong absorption line features because of small mismatches in resolution and tiny wavelength errors. The ratios of flux/continuum in Figure 2 display the nature of the absorption lines, and the irrelevant small mismatches at line centers are often off-scale and can be easily ignored. Longward of 1  $\mu\text{m}$ , the 2013 Kurucz model, normalized to the STIS flux in the 6800–7700 Å range, is chosen for the composite Sirius SED. Many of the weak STIS features which are <1% correspond to spectral features in the Kurucz model. To define the final composite Sirius SED below 1675 Å, an IUE spectrum is used after normalization to the STIS flux by multiplying by 1.28. The highest speed IUE trail data used for bright stars often missed the exact slit center, making the absolute flux low; but see Section 3.4 for verification of the 1.28 factor. The blue curve in Figure 2 is from EPK, while the Cohen et al. (1992a) reference SED is green. The Cohen SED for Sirius is part of the CWW standard star network (Cohen et al. 1992b, Cohen 2007).

The EPK curve (blue) is more than 10% low at places in the top two panels of Figure 2 but differs from the Kurucz extrapolation (red) by only a few percent in the bottom panel. The EPK fluxes are the zero-point SED from their table 4, as scaled up by their -1.368

---

<sup>4</sup><http://kurucz.harvard.edu/stars/SIRIUS/>

mag for Sirius. Below  $0.9\ \mu\text{m}$ , the EPK SED is based on the vintage absolute flux for 109 Vir from Tüg et al. (1977), as scaled to zero magnitude. Between  $0.9$  and  $9\ \mu\text{m}$ , EPK warp NICMOS and ISO measured flux distributions to match various photometry. From  $9.4$ – $35\ \mu\text{m}$ , the upward trend of the blue curve in Figure 2 reflects the EPK smooth adjustment of the CWW model to closely track the MSX absolute fluxes of Price et al. (2004, PPEM).

The normalized Kurucz model (red) agrees with the observed STIS flux (black) to better than  $\sim 1\%$  over most of the wavelength range in the middle panel of Figure 2. The original 1993 specially tailored Kurucz model<sup>5</sup> agrees with his 2013 update to  $<1\%$  longward of  $1800\ \text{\AA}$ ; and at shorter wavelengths, the update fits the observed flux significantly better. This precise agreement of STIS and model suggests that the modeled flux could represent the true stellar flux with a similar accuracy of  $\sim 1\%$  longward of  $1\ \mu\text{m}$ .

### 3.2. MSX Absolute IR Flux

Absolute IR flux measurements with direct reference to laboratory standards were pioneered from the ground by Selby et al. (1983), Blackwell et al. (1983), Mountain et al. (1985), and Booth et al. (1989). From space where the atmosphere does not cause complications, the SPIRIT III instrument on the Midcourse Space Experiment (MSX) provided pedigreed absolute mid-IR fluxes from emissive reference spheres (ERS) that were ejected and observed as point sources with fluxes based on lab data and basic physics. Preliminary MSX results appear in Cohen et al. (2001), while PPEM present a definitive final analysis. In their table 9, PPEM compare their new ERS based absolute fluxes to the ensemble average of a subset of the CWW network of standards. However, the uncertainties

---

<sup>5</sup><http://kurucz.harvard.edu/stars/SIRIUS/>



for each of the 4 MSX bands in that table 9 seem to be the internal statistical precision to which the MSX flux scale can be related to the CWW average scale. For the final MSX external uncertainties of the absolute flux measures, the 1.4% from the PPEM abstract is most appropriate. Larger uncertainties of 3–4% are quoted for the calculated ERS fluxes; but those values are reduced by an analysis of the band-to-band flux ratios, which constrain the sphere temperature. A minimum error bar arises from the two uncertainties of 2% attributed to  $\pm 1\%$  in the sphere radii and  $\pm 1\%$  in the distance to the ejected spheres. If each of the 5 ERS ejection events are independent, eg. the 1% radius error is random and not the same for all 5 released spheres, then the error-in-the-mean floor for each band is  $\sqrt{(4 + 4)/5} = 1.3\%$ , which is consistent with the adopted 1.4% in Table 3.

In addition to the systematic corrections to the global CWW flux scale, the CWW flux for Sirius itself was found to be offset by 1% low compared to the ensemble set of CWW program stars. Table 3 summarizes these results and includes the correction factors and final MSX in-band, effective fluxes (irradiance) for Sirius, where the negative corrections mean that the CWW flux is low and must be increased by the tabulated factors to agree with the MSX results. The fluxes in column 5 of Table 3 are the integral fluxes over the bandpass from table 2 of PPEM divided by the table 1 bandwidth of Cohen et al. (2001) times the correction in column 4 of Table 3. Multiplying this total CWW correction factor by the column 7 ratio of the green CWW to the red curve adopted for the IR extension of the HST/STIS fluxes in Figure 2 produces the ratio of MSX to the adopted IR flux. These ratios of MSX to HST/STIS are tabulated in the final column (8) of Table 3 and are plotted with their  $2\sigma$  error bars of 2.8% as the filled circles at the MSX isophotal wavelengths in Figure 2.

To normalize the Kurucz model to the MSX lab based absolute flux calibration, the illustrated normalization that is based on the 5556 Å Vega flux of Megessier (1995) would

be multiplied by the average of the four factors in the final column of Table 3. However to properly weight the visible and mid-IR absolute fluxes, a weighted average correction of  $0.9945 \pm 0.5\%$  includes the 5556 Å normalization at unit value  $\pm 0.7\%$  with a  $1/0.7^2$  weight along with the four IR corrections with their  $1/1.4^2$  weights. Equivalently, to establish a new HST flux scale that is based on Vega at 5556 Å, the Megessier value should be multiplied by 0.9945. A revised, MSX weighted value of  $3.46 \times 10^{-9} \times 0.9945 = 3.44 \times 10^{-9} \pm 0.5\%$  is adopted. (Coincidentally, this new value is the same as recommended by Hayes (1985).) The most significant deviation among the five absolute flux measures is for the MSX A band, where the 0.976 offset from Table 3 is improved by the 0.9945 factor to 0.982, i.e. a deviation from unity by  $1.8/1.4 = 1.3\sigma$ . The revised absolute normalization is within the uncertainty expectations of all five absolute flux measures from the visible to the mid-IR.

### 3.3. Linnell and Mészáros Models

While the Sirius flux is difficult to model in detail in the far-UV, where the line-blanketing is severe, other modeling efforts reproduce the visible–IR shape. Figure 3 compares the best efforts of Linnell et al. (2013 and private comm.) and of Mészáros et al. (2012 and private comm.) to the STIS fluxes by dividing by the same Kurucz continuum level as in Figure 2. The Linnell model shown in Figure 3 is slightly improved over the on-line SED. The small differences between the Kurucz and Mészáros models are probably due to different solar abundances and different updates to the synthesis code. Mészáros uses the Asplund et al. (2005) abundances and the F. Castelli version of the synthesis code, while Linnell uses the I. Hubeny line list and Synspec. The modeling of the Sirius IR SED is robust with all three independent models agreeing to better than  $\pm 1\%$ , which increases confidence that the adopted Sirius IR flux is accurate to 1%.

### 3.4. SOLSTICE Absolute UV Flux

Figure 4 shows that the absolute UV flux of Sirius that is defined by IUE and STIS is confirmed by the independent lab based calibration of Snow et al. (2013) for the SOLSTICE fluxes<sup>6</sup> (green) over their 1300–3000 Å range. These two measured absolute flux levels agree to  $\sim 3\%$ , as expected from the SOLSTICE/STIS comparison for three stars in Bohlin & Gordon (2014). The structure of the spectral features in the STIS data (black) at  $R \sim 500$  often matches the Kurucz  $R=500$  resolution model (red) longward of 1675 Å. The  $R \sim 250$  IUE data (black) below 1675 Å and the  $R \sim 100$  SOLSTICE SEDs also nicely track the flux level of the model, but the spectral structure is smoother than the  $R=500$  model. In general, the observed spectral structure is remarkably well reproduced by the theoretical modeling, even with the heavy UV line-blanketing.

## 4. RESULTS FOR VEGA

### 4.1. Dust Rings

Once Sirius is established as a primary flux standard, the flux of any other star is determined by just the brightness relative to Sirius. These signal ratios are free of errors in instrumental flux calibrations. For example, the ratio of Vega to Sirius is available for a few IR missions; and the total flux of Vega on the HST absolute flux scale is this ratio times the well-modeled flux of the primary IR standard, Sirius. Vega is a pole-on rapid rotator (Peterson et al. 2006) requiring a model with temperature zones in the 7900–10150 K range (Aufdenberg et al. 2006). However longward of 4000 Å, a single temperature Kurucz model at 9400 K fits the STIS SED to 1%, as discussed by Bohlin (2007). After subtracting this

---

<sup>6</sup><http://bdap.ipsl.fr/fondue/>

CALSPEC Kurucz model for the Vega photospheric flux ( $T_{\text{eff}} = 9400\text{ K}$ ,  $\log g = 3.90$ ,  $[M/H] = -0.5$ , Bohlin 2007), the remainder is the emission from the dust rings surrounding Vega, as shown in Figure 5. The photospheric Kurucz model that fits the STIS flux for Vega is the dotted line, which decreases steeply to less than the total dust emission beyond  $\sim 40\text{ }\mu\text{m}$ .

The measured ratios of Vega/Sirius include the four broadband MSX points of PPEM ( $\times$ ), i.e. the Vega flux from their table 3 divided by the Sirius flux from their table 2. The open circles in Figure 5 are from the IRAC ratios (Marengo et al. 2009) with their 1% error bars. The DIRBE data are from the electronic version of table 1 in Smith et al. (2004), while Neugebauer et al. (1984) review the IRAS data<sup>7</sup>. Three of the six DIRBE values (squares) in Figure 5 are low at 3.5, 12, and 60  $\mu\text{m}$ , even after correcting Sirius by 0.014 mag for other stars in the 42 arcmin DIRBE beam (Su et al. 2013, hereafter Su). The 3.5 and 12  $\mu\text{m}$  points are offscale in Figure 5, while the three DIRBE measures at 2.2, 4.9, and 25  $\mu\text{m}$  nicely track the other experimental results. The error bars on the DIRBE points are the rms scatter divided by the square root of the number of observations ( $N$ ); however, there is another quoted DIRBE uncertainty  $\langle err \rangle$  due to background fluctuations. What is not clear is whether or not  $\langle err \rangle$  should be reduced by  $\sqrt{N}$  to get total DIRBE uncertainties. The illustrated error bars for DIRBE, IRAC, MSX, and IRAS all include a 1% uncertainty for the Sirius flux combined in quadrature with the instrumental rms scatter.

Using interferometric techniques in the K band at 2.1  $\mu\text{m}$ , Absil et al. (2013) measure a  $1.26 \pm 0.27\%$  dust contribution with respect to the Vega photosphere. Similarly, Defrère et al. (2011) find a  $1.23 \pm 0.45\%$  contribution from small grains at the H band. These interferometric results are the filled black circles in Figure 5 and are independent of the Sirius SED.

---

<sup>7</sup><http://irsa.ipac.caltech.edu/cgi-bin/Gator/nph-dd>

Su models the dust with three rings at different temperatures: An inner hot ring of radius  $\sim 1.5''$  at 2400 K, a warm 170 K ring at  $2\text{--}3''$ , and a cold 50 K ring peaked at  $11\text{--}14''$ . For the data analyzed here, a 270 K blackbody fits the warm component better than the 170 K of Su, while 62 K is used for the cold dust. Planck blackbody curves for the three temperatures are normalized to the observed fluxes in Figure 5. Following Su, the three blackbody curves are truncated longward of the peak with a steep  $\lambda^{-x}$  decline, where  $x=2.8$ , 2.5, and 2.9, instead of the  $x=2$  for the Rayleigh–Jeans slope. The total emission from all three blackbody curves (black curve) falls within  $\sim 1\sigma$  of the observational data, except for a  $\sim 2\sigma$  deviation for the MSX  $14.65\ \mu\text{m}$  point and for the two offscale and the  $60\ \mu\text{m}$  DIRBE points.

The normalization of the three dust components is summarized in Table 4 and includes the ratio of the peak dust emission to photosphere in the final column. The sum of dust emission plus photosphere could be used as a standard star SED in the IR with a  $\sim 1\%$  photospheric uncertainty plus the tabulated uncertainty in the dust contribution. However, this total IR Vega flux is dependent on the observational aperture size, which compromises its practical utility as a standard star longward of  $1\ \mu\text{m}$ .

The Kurucz special photospheric models that do not include the dust contributions are in the CALSPEC database as `alpha_lyr_mod_001.fits` ( $T_{\text{eff}} = 9400\ \text{K}$ ,  $\log g = 3.90$ ,  $[M/H] = -0.5$ ) and `sirius_mod_001.fits` ( $T_{\text{eff}} = 9850\ \text{K}$ ,  $\log g = 4.30$ ,  $[M/H] = +0.4$ ).

#### 4.2. No *Hipparcos* Evidence for Variability of Vega

EPK reported that the *Hipparcos* photometry  $H_p$  (van Leeuwen et al. 1997) shows that Vega is a variable star. Those data are reviewed here with the conclusion that this apparent variability is most likely caused by saturation of the pulse counting electronics in

the image dissector photomultiplier tube. For the brightest stars, Figure 6 shows increasing differences between  $H_p$ <sup>8</sup> and the V mag (Johnson et al. 1966) for A and F stars. For example,  $H_p$  for Sirius is  $\sim 0.37$  mag too faint, while for stars fainter than  $V=1$ , the two magnitude measures are equal within  $\sim 0.02$ . For Vega, the *Hipparcos* 0.087 mag is 0.06 fainter than the standard Johnson value of  $V=0.03$ .

Figure 7 shows that the exact effect of the pulse pileup is sensitive to environmental conditions, eg. temperature, as the electronics attempt to discriminate between coincident pulses. Thus, the recorded count rate fluctuates the most for the brightest star, Sirius, where the rms scatter of the 160 separate measures is 0.051 mag. For Vega after removing a spurious 2.29 value, the rms of the remaining 102 values is 0.014 mag, i.e. considerably above the typical 0.004–0.005 mag rms of fainter stars, where the  $H_p$  photometry becomes linear.

EPK state that while the discrepant magnitude for Vega "... might be attributed to saturation effects, other, brighter stars do not show such discrepancies between V and  $H_p$ . Hence, we conclude that the faintness of Vega cannot be attributed to non-linearity in *Hipparcos*." This work demonstrates just the opposite: Brighter stars *are* discrepant and the faint  $H_p=0.087$  for Vega *is* caused by non-linearity. Furthermore, the apparent variability and gradual apparent brightening of the four brightest stars in Figure 7 is probably caused by slight variations in the exact level of pulse pileup in the detector. The *Hipparcos* photometry does not provide good evidence for the variability of Vega.

Constructive comments on preliminary drafts were provided by M. Bessel, S. Deustua, R. Kurucz, Sz. Mészáros, T. Rauch, and the referee. Primary support for this work was provided by NASA through the Space Telescope Science Institute, which is operated by

---

<sup>8</sup>[http://vizier.u-strasbg.fr/viz-bin/VizieR-3?-source=I/239/hip\\_main](http://vizier.u-strasbg.fr/viz-bin/VizieR-3?-source=I/239/hip_main)

AURA, Inc., under NASA contract NAS5-26555.

## REFERENCES

- Absil, et al. 2013, A&A, 555, A104
- Asplund, M., Grevesse, N., & Sauval, A. J. 2005, in ASP Conf. Ser. 336, Cosmic Abundances as Records of Stellar Evolution and Nucleosynthesis, ed. T. G. Barnes III & F. N. Bash (San Francisco, CA: ASP), 25
- Aufdenberg, et al. 2006, ApJ, 645, 664
- Beuermann, K., Burwitz, V., & Rauch, T. 2006, A&A, 458, 541
- Blackwell, D. E., Leggett, S. K., Petford, A.D., Mountain, C. M., & Selby M. J. 1983, MNRAS, 205, 897
- Bohlin, R. 1998, Instrument Science Report, STIS 98-01 (Baltimore: STScI)
- Bohlin, R. 2003, 2002 HST Calibration Workshop, eds. S. Arribas, A. Koekemoer, and B. Whitmore (Baltimore: STScI), p. 115
- Bohlin, R. C. 2007, in ASP Conf. Ser. 364, The Future of Photometric, Spectrophotometric, and Polarimetric Standardization, ed. C. Sterken (Ann Arbor, MI: Sheridan Books), 315
- Bohlin, R. C., & Gilliland, R. L. 2004, AJ, 127, 3508 (BG)
- Bohlin R. C., Gordon, K. D., Rieke, G. H., Ardila, D., Carey, S., Deustua, S., Engelbracht, C., Ferguson, H. C., Flanagan, K., Kalirai, J., Meixner, M., Noriega-Crespo, A., Su, K. Y. L., and Tremblay, P. E. 2011, AJ, 141, 173
- Bohlin, R. C., & Gordon, K. D. 2014, PASP, in preparation
- Bohlin, R. C., Savage, B. D., & Drake, J. F. 1978, ApJ, 224, 132
- Booth, A. J., Selby, M.J., Blackwell, D.E., Petford, A.D., & Arribas S. 1989, A&A, 218, 167



- Cohen, M. 2007, in ASP Conf. Ser. 364, The Future of Photometric, Spectrophotometric, and Polarimetric Standardization, ed. C. Sterken (Ann Arbor, MI: Sheridan Books), 333
- Cohen, M., Walker, R. G., Barlow, M. J., & Deacon, J. R. 1992a, AJ, 104, 1650
- Cohen, M., Walker, R. G., Jayaraman, S., & Barker, E. 2001, AJ, 121, 1180
- Cohen, M., Walker, R. G., & Witteborn, F. C. 1992b, AJ, 104, 2030
- Defrère, D., et al. 2011, A&A, 534, A5
- Engelke, C. W., Price, S. D., & Kraemer, K. E. 2010, AJ, 140, 1919 (EPK)
- Gianninas, A., Bergeron, P., & Ruiz, M. T. 2011, ApJ, 743, 138 (G11)
- Gilliland, R. L., Goudfrooij, P., & Kimble, R. A. 1999, PASP, 111, 1009 (GGK)
- Goudfrooij, P. & Bohlin, R. 2006, Instrument Science Report, STIS 2006-03, (Baltimore: STScI)
- Hayes, D. S. 1985, in Calibration of Fundamental Stellar Quantities, Proc. of IAU Symposium No. 111, eds. D. S. Hayes, L. E. Pasinetti, A. G. Davis Philip (Reidel: Dordrecht), p. 225
- Hernandez, S., et al. 2012, "STIS Instrument Handbook", Version 12.0, (Baltimore:STScI)
- Holberg, J. B., Barstow, M. A., Bruhweiler, F. C., Cruise, A. M., & Penny, A. J. 1998, ApJ, 497, 935
- Johnson, H. L., Iriarte, B., Mitchell, R. I., Wisniewski, W. Z. 1966, Comm. Lunar Plan. Lab., 4, 99
- Landolt, A. U. 1992, 104 340
- Landolt, A. U., & Uomoto, A. K. 2007, AJ, 133, 768
- Linnell, A. P., DeStefano, P., & Hubeny, I. 2013, AJ, 146, 68

- Marengo, M., et al. 2009, ApJ, 700, 1647
- Megessier, C. 1995, A&A, 296, 771
- Mészáros, Sz., et al. 2012, AJ, 144, 120
- Mountain, C. M., Selby, M. J., Leggett, S. K., Blackwell, D. E., & Petford A. D. 1985, , A&A, 151, 399
- Neugebauer, G., et al. 1984, ApJL, 278, L1
- Peterson, D. M., et al. 2006, Nature, 440, 896
- Price, S. D., Paxson, G., Engelke, C., & Murdock, T. L. 2004, AJ, 128, 889 (PPEM)
- Rauch, T., & Deetjen, J. L. 2003, in ASP Conf. Series, Vol. 288, Stellar Atmosphere Modeling, eds. I. Hubeny, D. Mihalas, & K. Werner, 103
- Rauch, T., Werner, K., Bohlin, R., & Kruk, J. W. 2013, A&A, 560, A106
- Selby, M. J., Mountain, C. M., Blackwell, D. E., Petford, A. D., & Leggett, S. K. 1983, MNRAS, 203, 795
- Smith, B. J., Price, S. D., & Baker, R. I. 2004, ApJS, 154, 673
- Snow, M., Reberac, A., Quemerais, E., Clarke, J., McClintock, W. E., & Woods, T. N. 2013, in ISSI Scientific Report Series, Vol. 13, Cross-Calibration of Far UV Spectra of Solar System Objects and the Heliosphere, eds. E. Quemerais, M. Snow, and R. M. Bonnet (New York:Springer), 191
- Stys, D. J., Bohlin, R. C. & Goudfrooij, P. 2004, Instrument Science Report, STIS 2004-04, (Baltimore:STScI)
- Su, K. Y. L., et al. 2013, ApJ, 763, 118 (Su)
- Tremblay, P. E., & Bergeron, P. 2009, ApJ, 696, 1755
- Tüg, H., White, N. M., & Lockwood, G. W. 1977, A&A, 61, 679

- van Leeuwen, F., Evans, D. W., Grenon, M., Grossmann, V., Mignard, F., & Perryman, M. A. C. 1997, *A&A*, 323, L61
- Werner, K., Deetjen, J. L., Dreizler, S., Nagel, T., Rauch, T., & Schuh, S. L. 2003, in *ASP Conf. Series*, Vol. 288, *Stellar Atmosphere Modeling*, eds. I. Hubeny, D. Mihalas, & K. Werner, 31

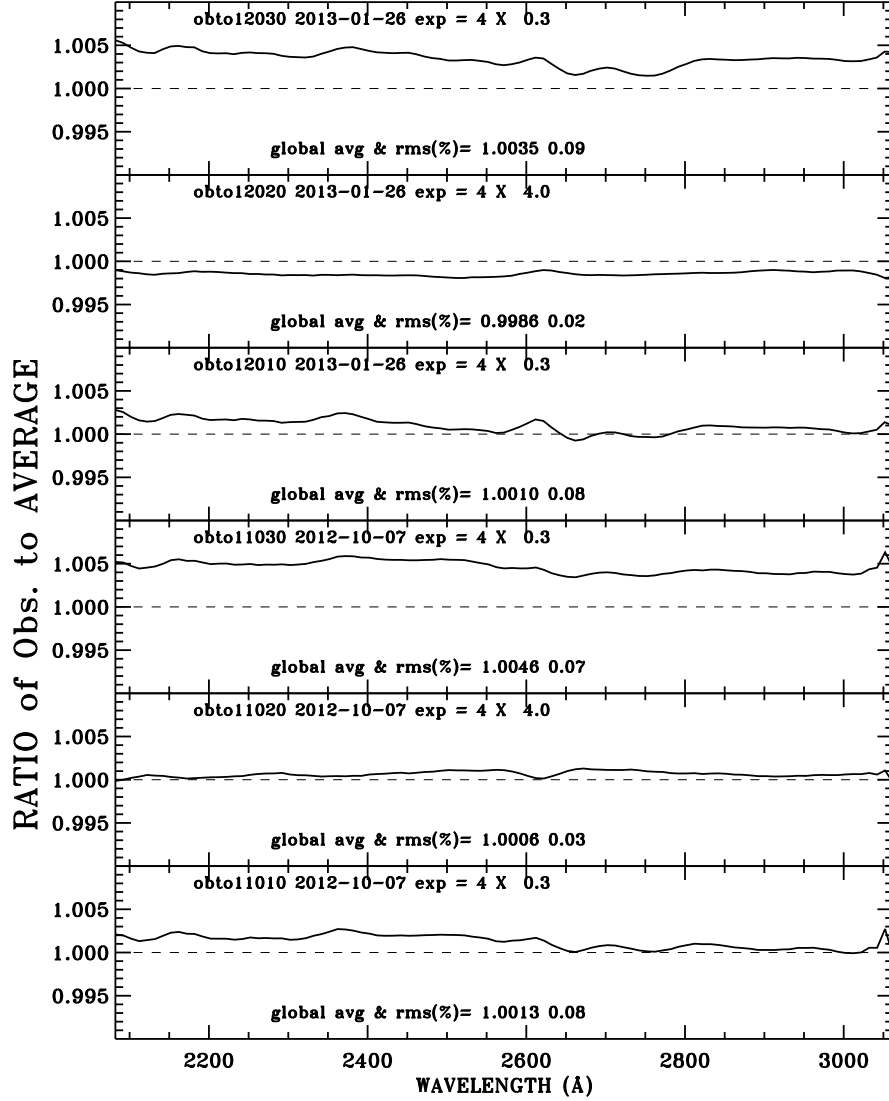


Fig. 1.— Ratios of each of the six observations of Sirius in the G230LB mode to the average of these six spectra. In addition to the exposure time of each of the CR-split=4 observations, the global average and rms of the residuals are written on the plots. The average spectrum is dominated by the two heavily saturated observations of 16s. Each independent observation repeats to  $\pm \sim 0.1\%$ , except for the last observation of each visit, which is high by  $\sim 0.4\%$ . The exposure time of the short observations is a small fraction of the total, so that this small non-repeatability has a  $< 0.1\%$  effect on the final average.

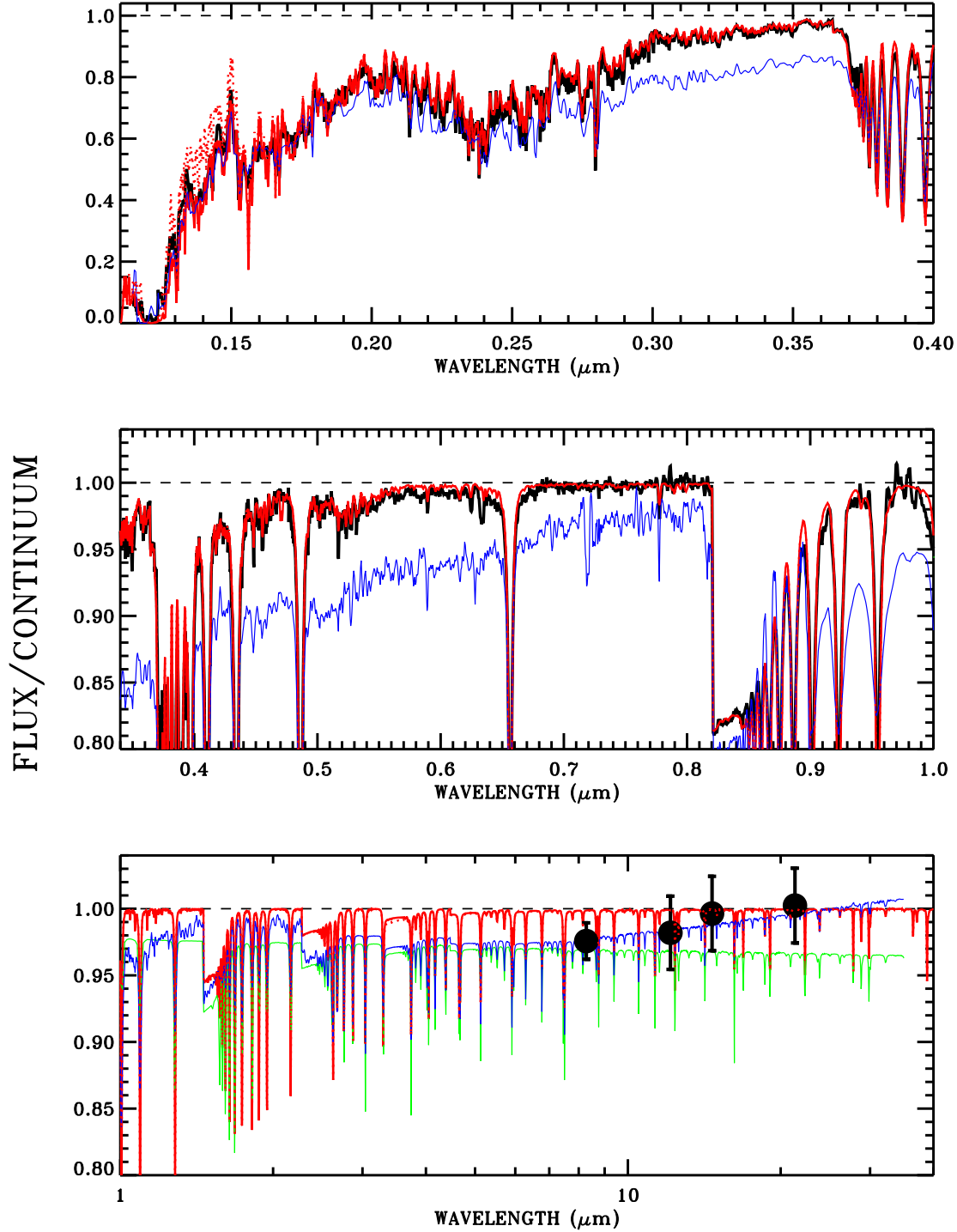


Fig. 2.— Comparison of STIS (black) to the Kurucz model (red: solid–2013 update, dots–original) with  $T_{\text{eff}} = 9850 \text{ K}$ ,  $\log g = 4.30$ , and  $[M/H] = +0.4$ . The original and 2013 Kurucz models coincide, except where the dots are discernable. The blue curve is from EPK, while green represents the CWW template for Sirius. The STIS data cover the wavelength range below  $1 \mu\text{m}$  and are supplemented by IUE data below  $1675 \text{ \AA}$ . The short wavelength limit of the CWW SED is  $1 \mu\text{m}$ . The black filled circles with  $2\sigma$  error bars are the MSX values of PPEM.

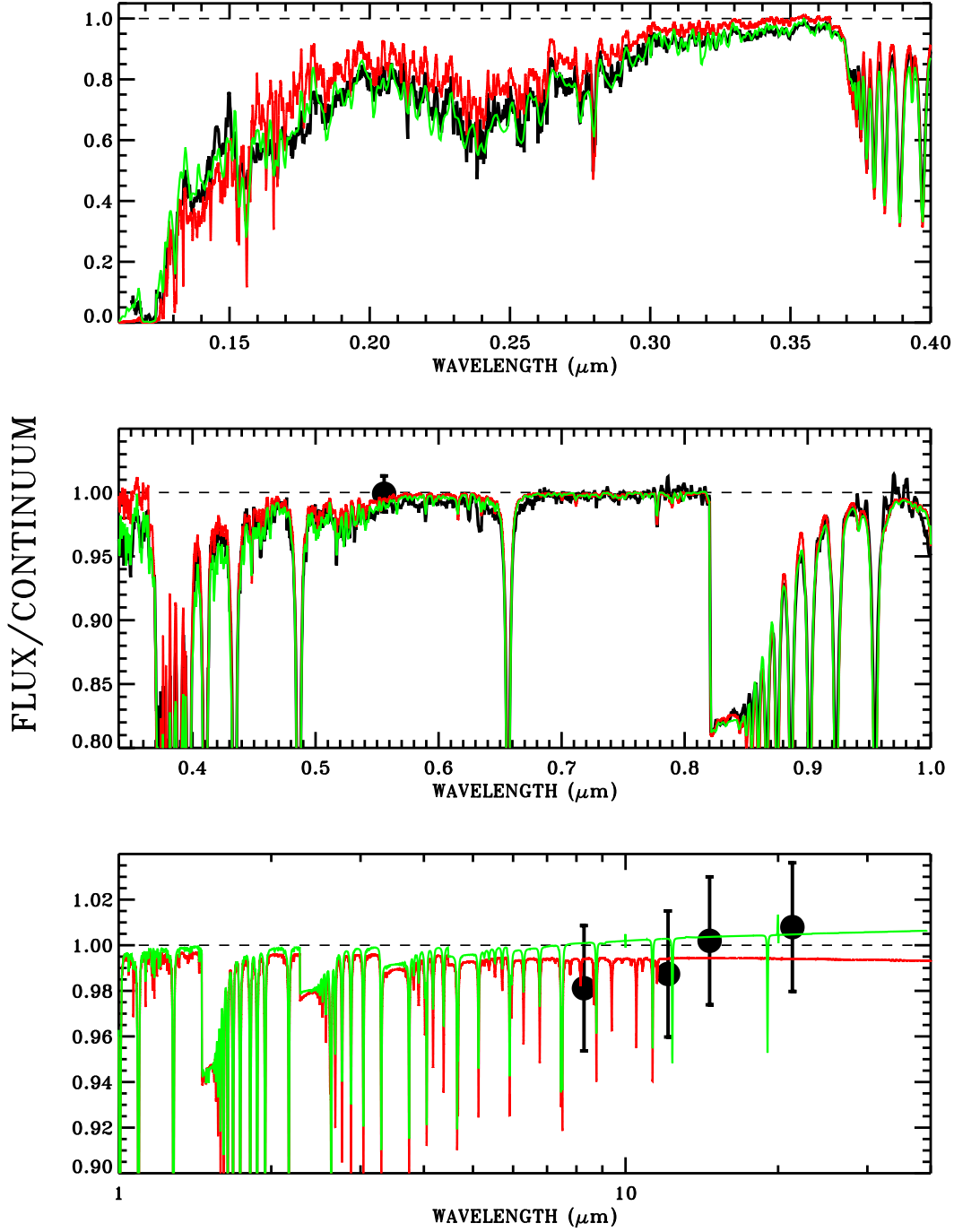


Fig. 3.— Comparison of STIS (black) to the best Sirius models by Linnell (green) and Mészáros (red), as in Figure 2. The black filled circles are the MSX values of PPDM but are now shown after the 0.9945 correction to the HST/STIS flux scale. The black circle at 0.556  $\mu\text{m}$  is the  $3.46 \times 10^{-9} \text{ erg cm}^{-2} \text{ s}^{-1} \text{ \AA}^{-1}$  value of Megessier (1995), which is now 0.55% above the STIS flux. Notice the expanded scale in the bottom panel, where both models are within 1% of the reference Kurucz model (red in Figure 2).

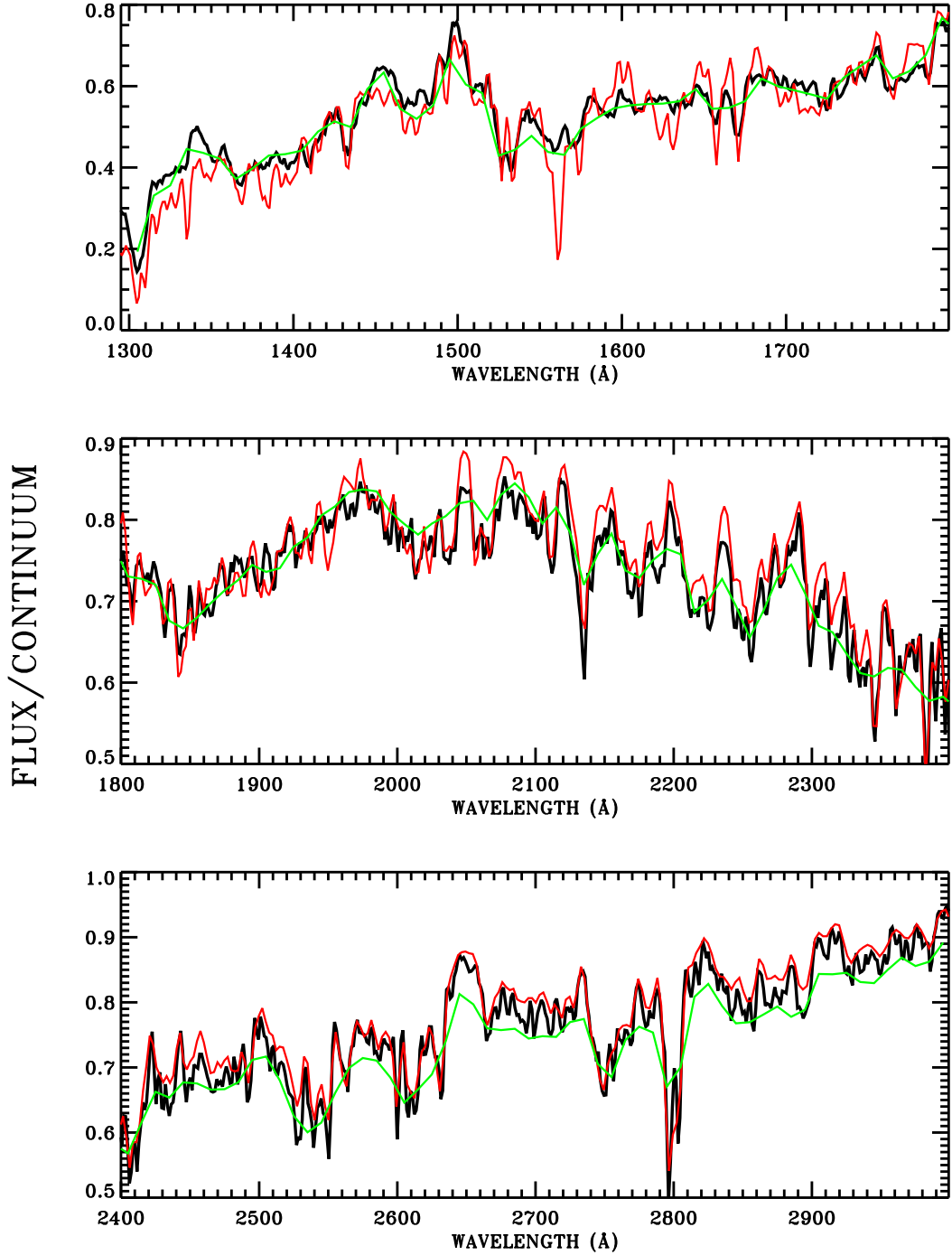


Fig. 4.— Comparison of STIS+IUE (black) and the Kurucz Sirius model (red) to the independent lab based SOLSTICE absolute fluxes (green), as in Figure 2. The two observational results agree to  $\sim 3\%$ , while the model tracks both observations with remarkable fidelity, considering the computational difficulty of accounting for the heavy line-blanketing at these UV wavelengths.

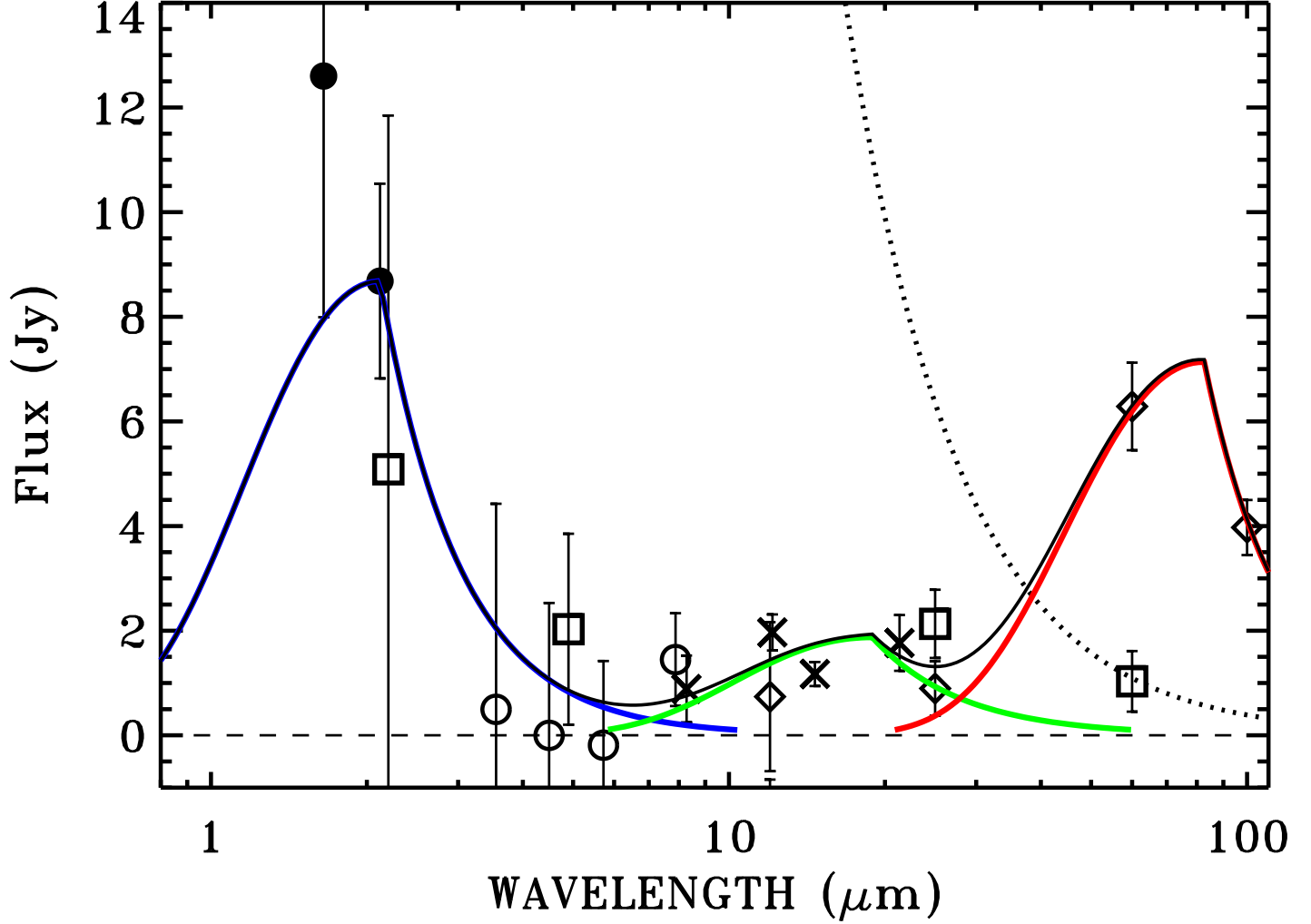


Fig. 5.— Emission from the Vega dust rings (data points and solid black line fit), which is the total flux minus the CALSPEC photospheric SED. The dotted line is the CALSPEC SED, i.e. the Kurucz photospheric model normalized to STIS at 6800–7700 Å. The data points with their  $1\sigma$  error bars are from various IR space missions: squares (DIRBE), open circles (IRAC),  $\times$  (MSX), diamonds (IRAS); and the filled circles are the ground-based interferometric results. The individual dust ring components are for 2400 K (blue), 270 K (green), and 62 K (red), while the continuous black line is the sum of these three components.



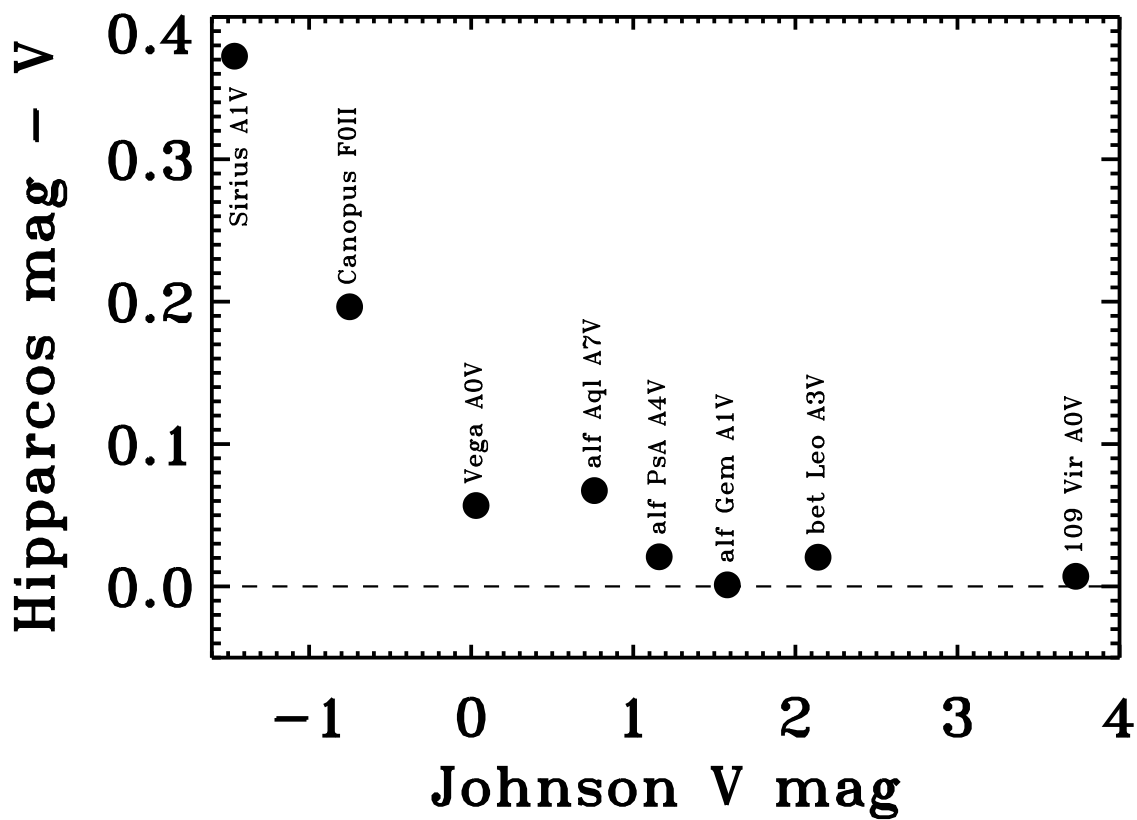


Fig. 6.— Non-linearity of *Hipparcos*  $H_p$  magnitudes for the brightest A and F stars.

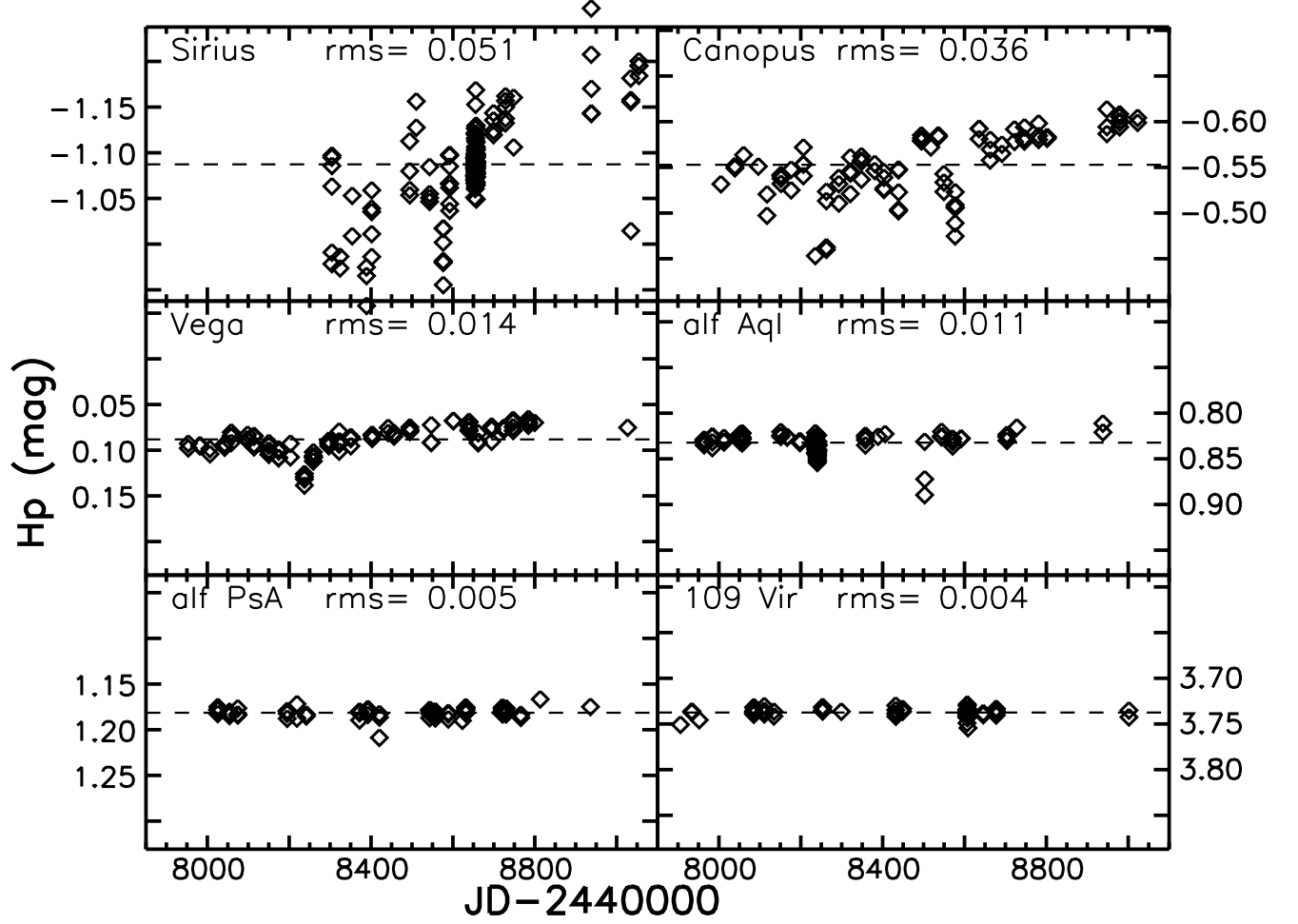


Fig. 7.— Apparent variability of *Hipparcos*  $H_p$  magnitudes for bright stars from a Johnson  $V$  mag of -1.46 for Sirius in the upper left panel to  $V=3.73$  for 109 Vir at the lower right. The brightest stars with  $V < 1$  in the top four panels are affected by instabilities at these highest count rates where pulse pileup is significant.

Table 1. Journal of STIS Observations in the 52X2 Arcsec Slit

Root	Mode	Date	Time	Exptime (s) <sup>a</sup>	Repeats
obto11010	G230LB	12-10-07	21:03:13	1.2	4
obto11020	G230LB	12-10-07	21:06:13	16.0	4
obto11030	G230LB	12-10-07	21:12:22	1.2	4
obto11040	G430L	12-10-07	21:23:12	0.9	3
obto11050	G430L	12-10-07	21:25:27	0.9	3
obto11060	G750L	12-10-07	21:35:32	2.1	7
obto12010	G230LB	13-01-26	12:10:59	1.2	4
obto12020	G230LB	13-01-26	12:13:59	16.0	4
obto12030	G230LB	13-01-26	12:20:08	1.2	4
obto12040	G430L	13-01-26	12:30:58	0.9	3
obto12050	G430L	13-01-26	12:33:13	0.9	3
obto12060	G750L	13-01-26	12:43:18	2.1	7

<sup>a</sup>Total exposure time. Individual sub-exposure integration times are this total divided by the number of repeats in the final column.

Table 2. The Primary WD Stars

Star	V <sup>a</sup>	Sp. T.	$T_{\text{eff}}$	$\log g$	Unc. $T_{\text{eff}}$
G191B2B	11.781	DA.8	59000	7.60	2000
GD153	13.346	DA1.2	40320	7.93	626
GD71	13.032	DA1.5	33590	7.93	483

<sup>a</sup>G191B2B–Landolt and Uomoto (2007), GD153–  
Landolt private comm, GD71–Landolt (1992)

Table 3. Sirius Flux Measured by MSX

Band ( $\mu\text{m}$ )	Corrections			Flux <sup>a</sup>	Uncert (%)	Corrections	
	Avg CWW (%)	Sirius (%)	Total CWW factor			CWW/HST factor	HST factor
8.28 (A)	+0.4	-1.0	1.006	8.477E-13	1.4	0.970	0.976
12.13 (C)	-0.4	-1.0	1.014	1.883E-13	1.4	0.968	0.982
14.65 (D)	-1.9	-1.0	1.030	9.031E-14	1.4	0.968	0.996
21.34 (E)	-2.5	-1.0	1.036	2.025E-14	1.4	0.967	1.002

<sup>a</sup> $\text{erg cm}^{-2} \text{ s}^{-1} \text{ \AA}^{-1}$

Table 4. Parameters of Vega Dust Model

$T_{\text{eff}}$ (K)	$\lambda_{\text{peak}}$ ( $\mu\text{m}$ )	Peak Flux (Jy)	Uncert (Jy)	Peak/Photos
2400	2.1	8.7	1.9	0.013
270	19	1.9	0.5	0.17
62	83	7.1	1.0	12.5